RSC Advances

ROYAL SOCIETY OF CHEMISTRY

www.rsc.org/advances

Journal Name

ARTICLE

Construction of Three-Dimensional $CuCo_2S_4$/CNT/graphene Nanocomposite for High Performance Supercapacitors

Received 00th January 20xx,
Accepted 00th January 20xx

DOI: 10.1039/x0xx00000x

www.rsc.org/

Jianfeng Shen[a,b], Jianhua Tang [a], Pei Dong[b], Zhuqing Zhang[a], Jin Ji[a], Robert Baines[b], Mingxin Ye[a]*

The search for safe and efficient energy storage systems continues to inspire researchers to develop new energy storage materials with excellent performance. Graphene-based three-dimensional (3D) nanostructures are interesting to supercapacitors (SCs) because of their high surface area, ample number of active sites, and good conductivity. This combination of attributes allows for full utilization capacitance of active electrode materials. Herein, three-dimensional $CuCo_2S_4$-g-CNT structure was fabricated successfully with the hydrothermal method. Serving as the active electrode, $CuCo_2S_4$-g-CNT demonstrated a remarkable specific capacitance (504 F g^{-1} at the current density of 10 A g^{-1}). Moreover, the as-obtained $CuCo_2S_4$-g-CNT hybrid electrode is robust, exhibiting exceptional cycle life, as revealed by galvanostatic charge-discharge studies (retaining 92.3% after 2000 cycles). Its durability is mainly due to the synergistic effects of $CuCo_2S_4$, graphene and CNTs. These unique nanoarchitectures demonstrate potential applications in energy storage electrodes and may indeed spur a new generation of hybrid SCs to bridge the energy gap between SCs and chemical batteries.

Introduction

As society rapidly develops, the need for high-performance energy storage devices has become more and more urgent. Supercapacitors (SCs) have acquired great attentions in the last few decades because of their high power density, super-long cycle life, and fast charging-discharging processes.[1-4] SCs can be classified into two types on the basis of their energy storage mechanism: electrical double layer capacitors (EDLCs) and pseudocapacitors. The electrode active materials are the most important factor in determining the properties of SCs.

Carbon materials, such as graphene and carbon nanotubes (CNTs), are commonly used for EDLCs because of their good electrical conductivity and large surface area.[5, 6] The charge storage mechanism for EDLCs is non-Faradaic, and no charge transfer across the electrode-electrolyte interface occurs during charging or discharging. Pseudocapacitors, on the other hand, provide relatively high specific capacitance and large energy density due to the reversible Faradaic reactions of the active materials.[7-10] Transition metal oxides, hydroxides, and sulfides have been widely investigated for use in pseudocapacitors since they provide multiple oxidation states for reversible Faradaic reactions.[11-16] It is now widely established that the benefits of EDLCs and pseudocapacitors can be simultaneously replicated by altering the nature of electrode active materials. Despite of the rapid progress, it is still vital and challenging to explore advanced electrode active materials with high capacitance, environmental friendliness and low cost.[8, 10, 17, 18]

Spinel structures containing binary or ternary metal oxides are also materials of interest for energy storage applications. Namely, spinel cobaltites (MCo_2O_4) are promising because they contain mixed valence metal cations that provide higher electronic conductivity and electrochemical activity in comparison with single-component oxides.[19-24] Among many kinds of electrode materials investigated for SCs, copper and cobalt-based materials are of particular interest.[9, 25-30] $CuCo_2O_4$, a binary metal oxide with higher electronic conductivity and electrochemical activity than single-component copper or cobalt oxides, has recently been thoroughly investigated.[31-37] On the other hand, graphene/mixed oxides composites have demonstrated encouraging electrochemical properties, which make them promising materials for high performance supercapacitors.[38, 39]

Motivated by the outstanding electrochemical performances of bimetallic oxides, bimetallic sulfides (such as Carrollite $CuCo_2S_4$) have emerged as a focus for the research community because they possess even higher electrical conductivities. They have been investigated for use as active electrode materials for high performance pseudocapacitors.[40-51] Although the conductivity of bimetal sulfides is better than that of their oxide counterparts, their capacitance performance is still limited.

The solution lies in nanostructured materials, specifically, constructing three-dimensional (3D) architectures based on two-dimensional (2D) substrates.[7, 52-54] Since pseudocapacitors only store charge in the first few nanometers from the surface, decreasing particle size can drastically increase the functionality of an active material. Therefore, the morphology and size of the active materials

[a] Institute of special materials and technology, Fudan University, 200433, Shanghai, China. E-mail:mxye@fudan.edu.cn
[b] Department of Materials Science and NanoEngineering, Rice University, 6100 Main Street, Houston, TX 77005, USA

Electronic Supplementary Information (ESI) available: [Detailed structural, morphological and supercapacitive properties characterization of $CoNi_2S_4$-g-CNT and its counterparts]. See DOI: 10.1039/x0xx00000x

play a vital role in determining their electrochemical performance and construction of nanostructures is of great significant for improving the supercapacitor performance. To this end, much attention has been given to the design and fabrication of three-dimensional (3D) nanostructures with large surface areas and short diffusion paths for electrons and ions. Therefore, it is crucial to retain a large contact area to fully maintain the advantages of active materials and to inhibit the volume change of these materials during cycling. Recently, constructing three-dimensional (3D) architectures based on two-dimensional (2D) substrates has been proven to be an effective approach to solve these problems.[7, 52-54]

Considering the aforementioned factors, we present the design and fabrication of 3D $CuCo_2S_4$-g-CNT. Comparing with recent developments for preparation of mixed oxides or sulfides,[38-41] our one-step method for preparation of $CuCo_2S_4$-g-CNT is low-cost and efficient, which forms $CuCo_2S_4$ nanoparticles and the 3D structure simultaneously. As far as we know, this is the first time report for $CuCo_2S_4$-based 3D nanocomposite.[35,36] Due to its compositional features and unique 3D structure, the $CuCo_2S_4$-g-CNT hybrid electrode exhibits significantly improved electrochemical performance, high areal capacitance, and good cyclic stability.

Experiments

Materials preparation

Single-walled CNTs (SWCNTs) were purchased from Shenzhen Nanotech Port Co., Ltd. (prepared with a chemical vapour deposition process with an average diameter of 4 nm and average length of 20~50 μm). Graphite was purchased from Qingdao BCSM. Co., Ltd. Doubly distilled water was used throughout the entire preparation process. All other chemicals were analytical level and used as received. The brief fabrication procedure for $CuCo_2S_4$-g-CNTs is illustrated in figure 1. The details for the procedure are as follows:

In the first step, graphite (150 milligrams) was mixed with 1:1 isopropanol (IPA)/water (50 mL) and sonicated at a frequency of 40 kHz for 4 h. Then, the mixture was centrifuged at 4000 r.p.m. for 20 min to obtain the stable supernatant.[55] In the second step, 1 mmol $CuCl_2 \cdot 2H_2O$, 2 mmol Co $(NO_3)_2 \cdot 6H_2O$, and 9 mmol thiourea were dissolved in a 50 mL stable graphene solution (IPA/water 1:1). 1 mL of ammonia and 25 mg SWCNTs were added to the solution, which was magnetically stirred and sonicated for 1 hour. Subsequently, we transferred the mixture into a Teflon-lined autoclave that was sealed and heated at 180 °C in an oven for 24 h. The acquired product was filtered and washed with water and ethanol, three times for each, and then dried in vacuum at 60 °C for 12h. As for $CuCo_2S_4$-g, 25, 50, and 100 mL of graphene solution (IPA/water 1:1) without CNTs were added respectively, to obtain $CuCo_2S_4$-g-1, $CuCo_2S_4$-g-2, and $CuCo_2S_4$-g-3.

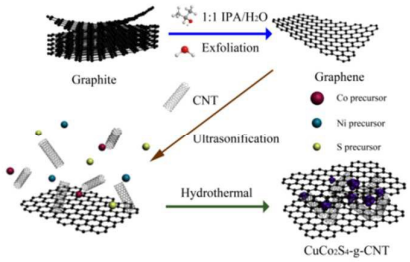

Figure 1. Process for preparation of $CuCo_2S_4$-g-CNT nanocomposite

Materials Characterization

We obtained wide-angle powder X-ray diffraction (XRD) patterns with a Rigaku D/MaxUltima II Powder XRD 6s, with monochromatic Cu Ka radiation (40 kV, 40 mA). The near-surface elemental composition of $CuCo_2S_4$-g-CNT was determined with X-ray photoelectron spectroscopy (XPS) (PHI Quantera X-ray photoelectron spectrometer). Binding energies were calibrated by referencing to C 1s (284.5 eV). Raman spectroscopy was recorded with a RENISHAW invia Raman Microscope at 532 nm laser excitation. Fourier transform infrared (FT-IR) spectra were characterized with Nicolet Is10. TGA was carried out using a NETZCH TG209, from ambient temperature to 600 ºC at a heating rate of 10 ºC/min, under nitrogen atomosphere. Nitrogen adsorption-desorption isotherms were carried out at 77 K with Micromeritics Tristar 3000 porosimeter.

The morphology of the samples was examined via scanning electron microscopy-energy dispersive spectroscopy (SEM-EDX) and transmission electron microscopy (TEM) (JEOL 2010). SEM images were collected with a FEI Quanta 400 ESEM FEG at an accelerating voltage of 5 kV and current of 10 A. UV-Vis diffusive reflectance spectra were performed with a Shimadzu UV-3600 spectrophotometer. We employed Autolab PGSTAT128N electrochemical workstation in both the two-electrode and three-electrode systems, using a 6 M KOH aqueous solution as electrolyte. Cyclic voltammetry (CV) curves were performed at various scan rates (5 to 100 mV s^{-1}) in a potential window of 0-0.6 V. Additionally, we attained Galvanostatic charge-discharge (GCD) curves at various current densities (1 to 20 A g^{-1}) in a potential window of 0-0.4 V.

Results and discussion

The X-ray diffraction (XRD) results of the prepared $CuCo_2S_4$-containing samples are illustrated in figure 2. Most of the diffraction peak characteristics (red lines) can be ascribed to the cubic phase of $CuCo2S_4$ (JCPDS No 24-334). In order to investigate the chemical and electronic states of $CuCo_2S_4$, X-ray photoelectron spectroscopy (XPS) and EDX measurements were conducted (figure S1 and S2).

As the results indicate, the ratios of Cu, Co, and S elements in $CuCo_2S_4$-g-CNT are 1:2.35:4.08 and 1:2.11:4.02, respectively, matching well with the formula of $CuCo_2S_4$. Raman, FTIR, and TGA ananlyses, which are consistent with XRD and XPS results, also confirm the composition and structures of these $CuCo_2S_4$-contaning samples.

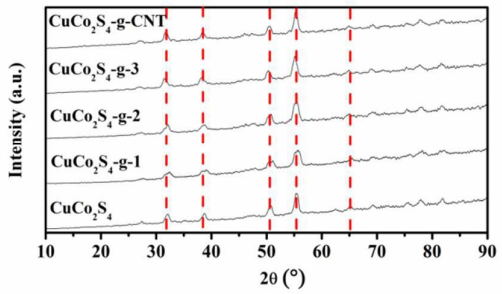

Figure 2. XRD patterns of $CuCo_2S_4$, $CuCo_2S_4$-g and $CuCo_2S_4$-g-CNT

The morphology of the as-prepared samples was revealed using SEM and TEM analyses. Typical clusters on graphene can be seen from the morphology of $CuCo_2S_4$ CNT (figure 3a). When the observation is magnified (figure 3b), a clear view of the sheets connected with CNTs becomes apparent. A more revealing feature of the $CuCo_2S_4$-g-CNT 3D structure can be seen from TEM analysis. As the TEM image displayed in figure 3c illustrates, most of the $CuCo_2S_4$, graphene, and CNTs are closely interwoven.

We further investigated the microstructure of $CuCo_2S_4$-g-CNT using HRTEM, as shown in figure 3d. HRTEM imaging of the edges of the graphene nanosheets indicates that its lattice fringes are oriented in the same direction, without any domain boundaries. Moreover, there are lucid lattice fringes for $CuCo_2S_4$ at 0.947 nm .[56] Clear stripes indicate that the as-prepared nanosheets are in single-crystalline structure.[57]

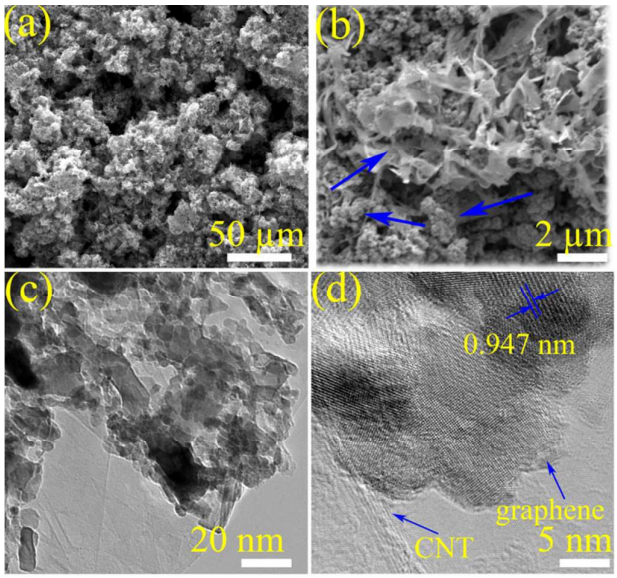

Figure 3. Low and high resolution SEM (a and b) and TEM images (c and d) of $CuCo_2S_4$-g-CNT.

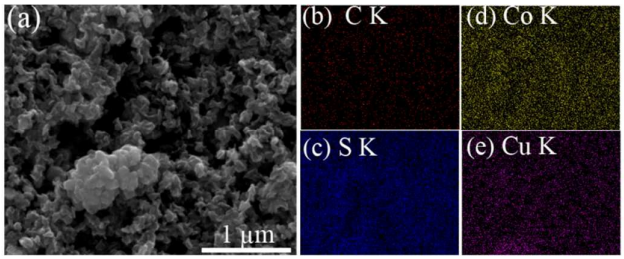

Figure 4. SEM-EDX mapping of $CuCo_2S_4$-g-CNT

To better understand the morphology and elemental distribution of $CuCo_2S_4$-g-CNT, SEM-EDX mapping was performed. (figure 4). The corresponding elemental mapping clearly shows the homogeneous distribution of Cu, Co, C and S throughout the entire sample.

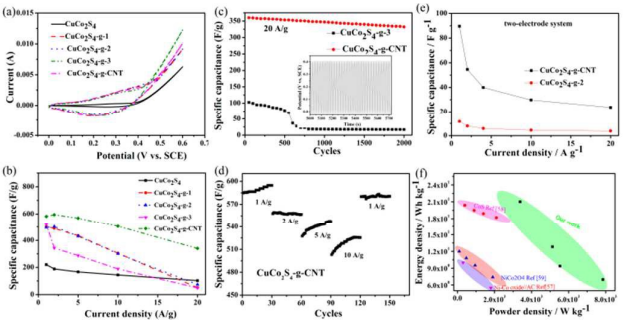

Figure 5. CV curves for $CuCo_2S_4$, $CuCo_2S_4$,-g and $CuCo_2S_4$,-g-CNT with scan rate of 5 mV/s (a), specific capacitance of $CuCo_2S_4$, $CuCo_2S_4$,-g, and $CuCo_2S_4$,-g-CNT at different current densities (b), specific capacitance of $CuCo_2S_4$,-g-3 and $CuCo_2S_4$,-g-CNT as a function of cycle number at a current density of 20A g^{-1} (c), cycle stability of $CuCo_2S_4$-g-CNT at different current densities (d), the specific capacitance of $CuCo_2S_4$-g-CNT and $CuCo_2S_4$-g-2 (e), and Ragone plots (f) of $CuCo_2S_4$-g-CNT based symmetric device.

To investigate the electrochemical performances of the as-synthesized $CuCo_2S_4$-g-CNTs nanosheets, CV and GCD were carried out using a three-electrode system in 6 M KOH solution. From CV measurements (figure S6 and figure 5a), it can be observed that a higher scan rate generally results in shorter redox times, leading to incomplete redox transitions at the "inner" active sites.[58] Clearly, compared with other $CuCo_2S_4$-based samples, $CuCo_2S_4$-g-CNT exhibits the highest capacitance. Based on the curves in figure 5, a pair of an integrated oxidation peak and reduction peak exists, implying the typical pseudocapacitive behaviour of the $CuCo_2S_4$-g-CNT. This result underscores the significance of optimizing both the crystallinity and 3D structure for improving energy-storage performance.

GCD data at various current densities, ranging from 1 to 20 A g^{-1} (figure 5b and figure S7), are consistent with CV data. The high capacitance of $CuCo_2S_4$-g-CNT is retained due to better charge transfer kinetics, as well as ion diffusion without the necessity of binder blocks. Current densities increase with corresponding decrease in specific capacitances.

Cycle stability is another indicator of electrochemical performance of a supercapacitor. For evaluation of the stability of the $CuCo_2S_4$-g-CNT electrode, the values of specific capacitance with respect to the cycle numbers at a current density of 20 A g^{-1} between 0 and 0.4 V were measured and compared with that of $CuCo_2S_4$-g-2 (figure 5c). The specific capacitance gradually decreased with an increase in the cycle number, and 89% of the initial specific capacitance was retained after 2000 cycles. Cycling stability is also evaluated through repeated charge-discharge measurements at progressively increasing current densities, and then at the original current density. As is shown in figure 5d, the specific capacitances of $CuCo_2S_4$-g-CNT increase during the first 120 cycles, which is possibly due to structural activation and pore opening of the sample during cycling test.[33] When the current density returns to 1A g^{-1} after the whole cycle, the specific capacity of $CuCo_2S_4$-g-CNT undergoes no obvious change. This illustrates the excellent electrochemical stability and rate capability of $CuCo_2S_4$-g-CNT. The electrochemical stability reveals that a highly reversible redox reaction occurred at the electrode without obvious phase change or structural damage to the active material (figure S8).

The $CuCo_2S_4$-g-CNT and $CuCo_2S_4$-g-2 coated Ni foam substrates were assembled in a two-electrode configuration with 6 M KOH as the electrolyte (symmetric cells in a parallel-plate geometry, which is typically used in SCs measurements). Their electrochemical behaviours were each characterized using CV at varying scan rates and GCD at several current densities, as shown in figure 5e, figure S9, and 10. For the $CuCo_2S_4$-g-CNT based device, both CV and GCD results indicate much higher capacities.

We further assessed the capabilities of $CuCo_2S_4$-g-CNT nanocomposite by conducting electrochemical impedance spectroscopy (performed in the frequency range of 0.01-10^5 Hz at open-circuit potential with an AC perturbation of 5 mV, figure S11). In the low-frequency region, there is a straight line for $CuCo_2S_4$-g-CNT. As well, compared to $CuCo_2S_4$-g, $CuCo_2S_4$-g-CNT's R_{ct} value is lower. These findings are indicative of excellent capacitive behaviour and conductivity. Energy density and power density are the two vital parameters to characterize the performances of SCs. Figure 5f shows the Ragone plots of the symmetric SC cell based on the GCD curves, which is higher than previous reports.[59-61] In order to investigate the surface properties of the as-prepared samples, nitrogen adsorption-desorption was measured. It is shown that the specific surface areas of $CuCo_2S_4$, $CuCo_2S_4$-g-2 and $CuCo_2S_4$-g-CNT are 6.163, 12.849 and 42.981 m^2 g^{-1}, respectively (Table S2). The higher BET specific surface area of $CuCo_2S_4$-g-CNT can offer more diffusion paths for the electrolyte transport, thus greatly improving the electrochemical performance.

The outstanding electrochemical performance of $CuCo_2S_4$-g-CNT can be attributed to the following factors. Foremost, its 3D structure is sufficiently porous and has a high specific surface area. This provides more active sites for electrochemical reactions and efficient penetration of ions. The high specific surface area also creates pathways for rapid transport of electrons and ions, even at high rates.[40] In general, reduction of specific capacitance at high rates is primarily attributed to low diffusion of electrolyte ions. Such is usually limited by diffusion due to the time constraint during high-rate charge-discharge processes. The 3D structure of $CuCo_2S_4$-g-CNT provides a short path length high accessibility for the electrolyte, effectively improving the pseudo capacitance of $CuCo_2S_4$ at high rates.[62] Secondly, the high conductivity of 3D $CuCo_2S_4$-g-CNT decreases the resistance, enhancing the rate performance of the electrode materials (figure S12).[17] Finally, the high conductivity of $CuCo_2S_4$-g-CNT 3D structure facilitates electron transfer, which disposes it to quick charge-discharge cycles.

Conclusions

In this work, the ternary component of $CuCo_2S_4$-g-CNT was prepared for the first time. We attribute the marvellous electrochemical performance of $CuCo_2S_4$-g-CNT to its unique nanostructure consisting of a highly conductive graphene/CNT network and stable three-dimensional architecture. The 3D nanostructure is extremely stable during long-life charging-discharging processes. As a result, it demonstrates dramatic improvement in capability and cycling. When evaluated as an active material, $CuCo_2S_4$-g-CNT exhibits high specific capacitance and excellent cyclic stability. Its 3D nanostructure, consisting of graphene and $CuCo_2S_4$ connected with CNTs, not only addresses the aggregation of nanoparticles but also facilitates faster charge transport and buffers the volume change during cycling. In sum, the synergetic effect among ternary components makes $CuCo_2S_4$-g-CNT a promising electrode material for SC applications.

Acknowledgements

This work was financially supported by National Natural Science Foundation of China (51202034).

Notes and references

1. T. M. Higgins, D. McAteer, J. C. M. Coelho, B. M. Sanchez, Z. Gholamvand, G. Moriarty, N. McEvoy, N. C. Berner, G. S. Duesberg, V. Nicolosi and J. N. Coleman, *ACS Nano*, 2014, **8**, 9567-9579.
2. Y. Yan, Q. Cheng, V. Pavlinek, P. Saha and C. Li, *Electrochim. Acta*, 2012, **71**, 27-32.
3. W. Tang, L. Peng, C. Yuan, J. Wang, S. Mo, C. Zhao, Y. Yu, Y. Min and A. J. Epstein, *Synth. Met.*, 2015, **202**, 140-146.
4. R. B. Rakhi, W. Chen, D. Cha and H. N. Alshareef, *Adv. Energy Mater.*, 2012, **2**, 381-389.
5. L. Fan, G. Liu, C. Zhang, J. Wu and Y. Wei, *Int. J. Hydrogen Energy*, 2015, **40**, 10150-10157.
6. W. Du, Z. Wang, Z. Zhu, S. Hu, X. Zhu, Y. Shi, H. Pang and X. Qian, *J. Mater. Chem. A*, 2014, **2**, 9613-9619.
7. S. K. Balasingam, J. S. Lee and Y. Jun, *Dalton T.*, 2015, **44**, 15491-15498.

8. H. Jiang, Y. Dai, Y. Hu, W. Chen and C. Li, *ACS Sustain. Chem. Eng.*,, 2014, **2**, 70-74.
9. M. Liu, L. Kong, C. Lu, X. Li, Y. Luo and L. Kang, *ACS Appl. Mater. Interfaces.*, 2012, **4**, 4631-4636.
10. J. Tao, N. Liu, W. Ma, L. Ding, L. Li, J. Su and Y. Gao, *Sci. Rep.*, 2013, **3**, 2286.
11. K. Xu, Q. Ren, Q. Liu, W. Li, R. Zou and J. Hu, *RSC Adv.*,
2015, **5**, 44642-44647.
12. W. Cai, T. Lai, W. Dai and J. Ye, *J. Power Sources*, 2014, **255**, 170-178.
13. X. Wang, B. Liu, R. Liu, Q. Wang, X. Hou, D. Chen, R. Wang and G. Shen, *Angew. Chem. Int. Edit.*, 2014, **53**, 1849-1853.
14. H. Wan, J. Liu, Y. Ruan, L. Lv, L. Peng, X. Ji, L. Miao and J. Jiang, *ACS Appl. Mater. Interfaces.*, 2015, **7**, 15840-15847.
15. L. Yu, G. Zhang, C. Yuan and X. W. Lou, *Chem. Commun.*, 2013, **49**, 137-139.
16. W. Yang, Z. Gao, J. Ma, X. Zhang, J. Wang and J. Liu, *J. Mater. Chem. A*, 2014, **2**, 1448-1457.
17. Y. Zhu, Z. Wu, M. Jing, X. Yang, W. Song and X. Ji, *J. Power Sources*, 2015, **273**, 584-590.
18. Y. Xiao, Y. Lei, B. Zheng, L. Gu, Y. Wang and D. Xiao, *RSC Adv.*, 2015, **5**, 21604-21613.
19. S. Peng, L. Li, H. B. Wu, S. Madhavi and X. W. Lou, *Adv.*
Energy. Mater., 2015, **5**, 1401172.
20. M. Liu, L. Kong, C. Lu, X. Ma, X. Li, Y. Luo and L. Kang, *J. Mater. Chem. A*, 2013, **1**, 1380-1387.
21. L. Mai, F. Yang, Y. Zhao, X. Xu, L. Xu and Y. Luo, *Nat. Commun.*, 2011, **2**, 381.
22. S. Chen and S. Qiao, *ACS Nano*, 2013, **7**, 10190-10196.
23. M. N. Patel, X. Wang, D. A. Slanac, D. A. Ferrer, S. Dai, K. P. Johnston and K. J. Stevenson, *J. Mater. Chem.*, 2012, **22**, 3160-3169.
24. L. Huang, D. Chen, Y. Ding, Z. L. Wang, Z. Zeng and M. Liu, *ACS Appl. Mater. Interfaces.*, 2013, **5**, 11159-11162.
25. Y. Chen, B. Liu, Q. Liu, J. Wang, J. Liu, H. Zhang, S. Hu and X. Jing, *Electrochim. Acta*, 2015, **178**, 429-438.
26. J. Yang, M. Ma, C. Sun, Y. Zhang, W. Huang and X. Dong, *J. Mater. Chem. A*, 2015, **3**, 1258-1264.
27. V. H. Nguyen and J.-J. Shim, *Electrochim. Acta*, 2015, **166**, 302-309.
28. D. Guo, P. Zhang, H. Zhang, X. Yu, J. Zhu, Q. Li and T. Wang, *J. Mater. Chem. A*, 2013, **1**, 9024-9027.
29. C. Yuan, J. Li, L. Hou, J. Lin, X. Zhang and S. Xiong, *J. Mater. Chem. A*, 2013, **1**, 11145-11151.
30. L. Niu, Z. Li, Y. Xu, J. Sun, W. Hong, X. Liu, J. Wang and S. Yang, *ACS Appl. Mater. Interfaces.*, 2013, **5**, 8044-8052.
31. Q. Wang , J. Xu, X. Wang, B. Liu, X. Hou, G. Yu, P. Wang, D. Chen and G. Shen, *ChemElectroChem*, 2014, **1**, 559-564.
32. S. Gu, Z. Lou, X. Ma and G. Shen, *ChemElectroChem*, 2015, **2**, 1042-1047.
33. A. Pendashteh, M. S. Rahmanifar, R. B. Kaner and M. F. Mousavi, *Chem. Commun.*, 2014, **50**, 1972-1975.
34. H. Chen, X. Chen, Y. Zeng, S. Chen and J. Wang, *RSC Adv.*, 2015, **5**, 70494-70497.
35. K. Zhang, W. Zeng, G. Zhang, S. Hou, F. Wang, T. Wang and H. Duan, *RSC Adv.*, 2015, **5**, 69636-69641.
36. A. Pendashteh, S. E. Moosavifard, M. S. Rahmanifar, Y. Wang, M. F. El-Kady, R. B. Kaner and M. F. Mousavi, *Chem. Mater.*, 2015, **27**, 3919-3926.
37. R. Ning, J. Tian, A. M. Asiri, A. H. Qusti, A. O. Al-Youbi and X. Sun, *Langmuir*, 2013, **29**, 13146-13151.
38. B. Li, Y. Fu, H. Xia and X. Wang, *Mater. Lett.*, 2014, **122**,
193-196.
39. H. Xia, C. Hong, B. Li, B. Zhao, Z. Lin, M. Zheng, S. V. Savilov and S. M. Aldoshin, *Adv.Funct. Mater.*, 2015, **25**, 627-635.
40. T. Peng, Z. Qian, J. Wang, D. Song, J. Liu, Q. Liu and P. Wang, *J. Mater. Chem. A*, 2014, **2**, 19376-19382.
41. X. Xiong, G. Waller, D. Ding, D. Chen, B. Rainwater, B. Zhao, Z. Wang and M. Liu, *Nano Energy*, 2015, **16**, 71-80.
42. J. Xiao, L. Wan, S. Yang, F. Xiao and S. Wang, *Nano Lett.*, 2014, **14**, 831-838.
43. A. N. Buckley, W. M. Skinner, S. L. Harmer, A. Pring and L. Fan, *Geochimica et Cosmochimica Acta*, 2009, **73**, 4452-4467.
44. L. Mei, T. Yang, C. Xu, M. Zhang, L. Chen, Q. Li and T. Wang, *Nano Energy*, 2014, **3**, 36-45.
45. Z. Wu, X. Pu, X. Ji, Y. Zhu, M. Jing, Q. Chen and F. Jiao, *Electrochim. Acta*, 2015, **174**, 238-245.
46. S. Peng, L. Li, C. Li, H. Tan, R. Cai, H. Yu, S. Mhaisalkar,
M. Srinivasan, S. Ramakrishna and Q. Yan, *Chem. Commun.*, 2013, **49**, 10178-10180.
47. J. Tang, J. Shen, N. Li and M. Ye, *Ceram. Int.*, 2015, **41**, 6203-6211.
48. L. Chen, Y. Zhou, H. Dai, T. Yu, J. Liu and Z. Zou, *Nano Energy*, 2015, **11**, 697-703.
49. W. Du, Z. Zhu, Y. Wang, J. Liu, W. Yang, X. Qian and H.
Pang, *RSC Adv.*, 2014, **4**, 6998-7002.
50. Z. Yang, X. Zhu, K. Wang, G. Ma, H. Cheng and F. Xu, *Appl. Surf. Sci.*, 2015, **347**, 690-695.
51. Y. Zhang, M. Ma, J. Yang, C. Sun, H. Su, W. Huang and X. Dong, *Nanoscale*, 2014, **6**, 9824-9830.
52. K. Byungwoo, C. Haegeun and K. Woong, *Nanotechnology*, 2012, **23**, 155401.
53. H. Wan, J. Jiang, J. Yu, K. Xu, L. Miao, L. Zhang, H.

Chen and Y. Ruan, *CrystEngComm*, 2013, **15**, 7649-7651.
54. C. Tan and H. Zhang, *Chem. Soc. Rev.*, 2015, **44**, 2713-2731.
55. J. Shen, Y. He, J. Wu, C. Gao, K. Keyshar, X. Zhang, Y. Yang, M. Ye, R. Vajtai, J. Lou and P. M. Ajayan, *Nano Lett.*, 2015, **15**, 5449-5454.
56. T. Oda, M. Shirai, N. Suzuki and K. Motizuki, *J. Phys-Condens. Mat.*, 1995, **7**, 4433.
57. H. Wang, C. Wang, C. Qing, D. Sun, B. Wang, G. Qu, M. Sun and Y. Tang, *Electrochim. Acta*, 2015, **174**, 1104-1112.
58. M. B. Zakaria, M. Hu, R. R. Salunkhe, M. Pramanik, K. Takai, V. Malgras, S. Choi, S. X. Dou, J. H. Kim, M. Imura, S. Ishihara and Y. Yamauchi, *Chem. – A Eur. J.*, 2015, **21**, 3605-3612.
597. Q. T. Qu, Y. Shi, S. Tian, Y. H. Chen, Y. P. Wu and R. Holze, J. Power Sources, 2009, **194**, 1222-1225.
60. F. Luo, J. Li, H. Yuan and D. Xiao, Electrochim. Acta, 2014, **123**, 183-189.
61. C. Yuan, J. Li, L. Hou, X. Zhang, L. Shen and X. W. Lou, Adv. Funct. Mater., 2012, **22**, 4592-4597.
62. H. Chen, J. Jiang, L. Zhang, H. Wan, T. Qi and D. Xia, Nanoscale, 2013, **5**, 8879-8883.

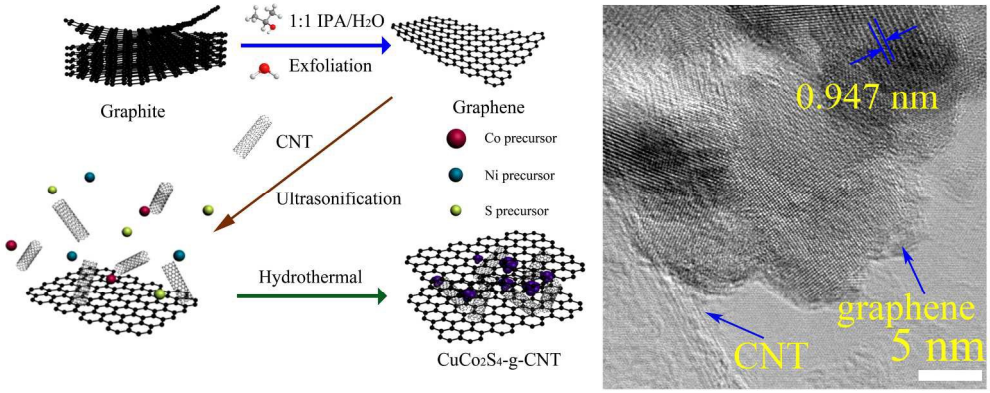

223x88mm (300 x 300 DPI)